



OPEN Morphological and functional analysis of colorectal cancer cell lines in 2D and 3D culture models

Seiichi Shinji^{1,2}✉, Yutaro Ogawa¹, Takeshi Yamada¹, Akihisa Matsuda¹, Kay Uehara¹, Yasuyuki Yokoyama¹, Goro Takahashi¹, Takuma Iwai¹, Toshimitsu Miyasaka¹, Shintaro Kanaka¹, Koki Hayashi¹, Yuuki Shichi², Masakazu Fujiwara², Kimimasa Takahashi³, Tomio Arai⁴, Toshiyuki Ishiwata² & Hiroshi Yoshida¹

The epithelial and mesenchymal features of colorectal adenocarcinoma (CRAC) cell lines were compared in two-dimensional (2D) and three-dimensional (3D) cultures. In 2D cultures, the three CRAC cell lines exhibited epithelial characteristics with high E-cadherin and low vimentin levels, whereas two exhibited mesenchymal traits with opposite expression patterns. In 3D cultures using low-attachment plates, mesenchymal cells from 2D cultures showed reduced vimentin mRNA levels. Morphologically, the five CRAC cell lines appeared similarly shaped in 2D culture but formed different structures in 3D culture. Epithelial DLD-1 and mesenchymal COLO-320 cells produced large granular spheres, whereas epithelial HCT-15 cells formed small solid spheres. Tubular structures were observed in epithelial CACO-2 and mesenchymal SW480 spheres. Desmosome-like structures developed in epithelial CRAC cells, whereas entosis was observed in CACO-2, HCT-15, and SW480 cells. The Ki-67-positive proliferating cell count varied in 2D and 3D cultures of epithelial cells but remained high and unchanged in mesenchymal cells. These findings suggest that while CRAC cells display distinct epithelial and mesenchymal properties in 2D cultures, they form diverse 3D structures, irrespective of these traits.

Keywords Colorectal adenocarcinoma, 2-dimensional culture, 3-dimensional culture, Sphere, Scanning electron microscopy, Transmission electron microscopy

Colorectal cancer (CRC) was the third most common cancer worldwide and the second leading cause of cancer-related deaths according to the International Agency for Research on Cancer (IARC) in 2018¹. CRC presents diverse molecular pathways and clinical presentations, and is now recognized as a heterogeneous disease. The patterns of CRC pathogenesis are heterogeneous, with the traditional adenoma-carcinoma sequence accounting for the majority of cases, and approximately 25% of CRCs arise from serrated precursor lesions^{2,3}. Furthermore, the recent demographic landscape of CRC has exhibited a shifted age distribution. The incidence rate of CRC among populations under the age of 50 is increasing⁴. Although projections suggest that by 2050, 6.9 million new patients over the age of 80 years (20.5% of all cancer cases) will be diagnosed with CRC worldwide⁵, the American Cancer Society (ACS) lowered the recommended age for average-risk CRC screening from 50 to 45 years^{6–8}. This dual trend underscores the need for tailored prevention and treatment strategies to address the growing diversity of CRC patient populations⁹.

Epithelial-mesenchymal transition (EMT) and mesenchymal-epithelial transition (MET) are biological processes that transform epithelial cells into mesenchymal cells and vice versa. These processes alter cell shape and structure, function, mobility, and malignant behaviors^{10–12}. In colorectal cancer, EMT plays an important role in increasing the aggressiveness and metastatic potential of tumor cells by giving cancer cells the ability to leave the primary tumor and spread to other tissues and organs¹³. Patients positive for the mesenchymal marker vimentin and negative for the epithelial marker E-cadherin possess a significantly higher tumor grade, tumor budding, invasive tumor front, and lymph node metastasis^{14,15}. E-cadherin expression in colorectal cancer

¹Department of Gastroenterological Surgery, Nippon Medical School, 1-1-5 Sendagi, Bunkyo-ku, Tokyo 113-8603, Japan. ²Division of Aging and Carcinogenesis, Research Team for Geriatric Pathology, Tokyo Metropolitan Institute for Geriatrics and Gerontology, 35-2 Sakae-cho, Itabashi-ku, Tokyo 173-0015, Japan. ³Department of Veterinary Pathology, School of Veterinary Medicine, Nippon Veterinary and Life Science University, Tokyo 180-8602, Japan. ⁴Department of Pathology, Tokyo Metropolitan Institute for Geriatrics and Gerontology, 35-2 Sakae-cho, Itabashi-ku, Tokyo 173-0015, Japan. ✉email: s-shinji@nms.ac.jp

cells may serve as a predictive marker of chemotherapeutic efficacy, potentially improving the effectiveness of conventional treatments¹⁶.

Transcriptional profile analyses have revealed that pancreatic ductal adenocarcinoma (PDAC) cells can be classified into two types: the classical type, in which adhesion-associated and epithelial genes are highly expressed, and the quasi-mesenchymal type, in which mesenchymal-associated genes are highly expressed¹⁷. We also reported that PDAC cell lines were classified as epithelial cells with high E-cadherin and low vimentin levels and mesenchymal cells with low E-cadherin and high vimentin^{18–20}. Epithelial pancreatic cancer cell lines in 3D culture are small and form spheres covered with flat-lining cells, whereas the spheres of mesenchymal pancreatic cancer cell lines are large, loosely bound, and cluster-like in shape. Epithelial and mesenchymal PDAC cells exhibit different cell proliferation as well as differences in the ability of spheres to adhere and spread on the culture plate^{20,21}. Heterogeneity in cancer cells is recognized as an important factor governing the characteristics and behavior of pancreatic cancer.

In this study, we examined the diversity of colorectal adenocarcinoma (CRAC) cell lines and found that they can be divided into epithelial and mesenchymal cells based on their identification markers, E-cadherin and vimentin. We identified heterogeneity among the CRAC cell lines in E-cadherin/vimentin expression, spherical morphology, and cell proliferative ability in 3D culture, suggesting that our 3D culture is a suitable model for the analysis of heterogeneous colon cancer.

Results

Quantitative reverse transcription-polymerase chain reaction (qRT-PCR) analysis

To clarify the epithelial and mesenchymal features of CRAC cells under 2D and 3D culture conditions, we examined the mRNA levels of the epithelial cell marker E-cadherin and the mesenchymal marker vimentin in five CRAC cell lines (DLD-1, CACO-2, HCT-15, SW480, and COLO-320) (Supplementary Figure S1). In 2D cultures, E-cadherin mRNA expression levels were in the following order of highest to lowest: DLD-1, CACO-2, HCT-15, SW480, and COLO-320. Under 2D culture conditions, DLD-1, CACO-2 and HCT-15 cells showed high E-cadherin and low vimentin mRNA levels, whereas SW480 and COLO-320 cells showed low E-cadherin and high vimentin mRNA levels (Fig. 1a, b, black bars). Taking the value of 2D-cultured COLO-320 cells as 1, DLD-1 cells had approximately 16,000-fold higher E-cadherin mRNA and less than one in six thousand the amount of vimentin mRNA expressed (black bars). When these CRAC cells are cultured on low-attachment plates, they form spheres that float and proliferate into cancer cell masses in the culture medium. In this 3D culture, DLD-1 cells, which showed the highest E-cadherin mRNA expression in the 2D culture, showed a statistically significant decrease in E-cadherin expression (Fig. 1a, white bars, $p < 0.05$). COLO320 and SW480 cells, which had the highest and second-highest vimentin expression in 2D culture, respectively, showed significantly decreased vimentin expression in 3D culture (Fig. 1b, white bars, $p < 0.05$).

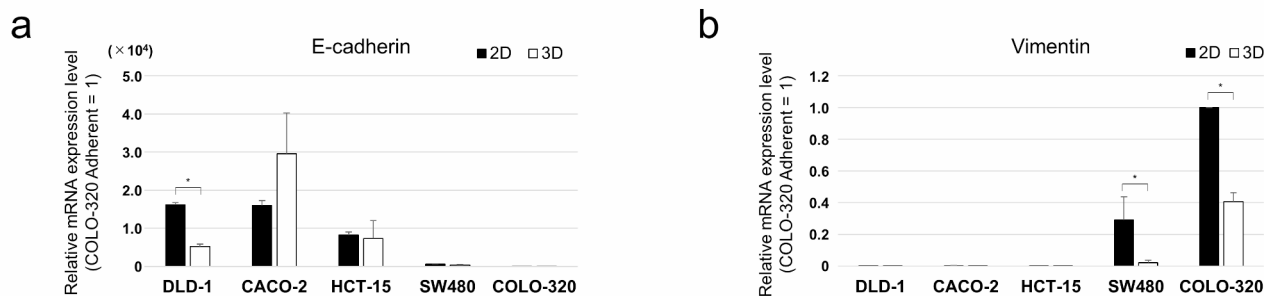


Fig. 1. E-cadherin and vimentin mRNA expression in 2D and 3D cultured colorectal adenocarcinoma (CRAC) cell lines. **(a)** E-cadherin and **(b)** vimentin mRNA levels were examined using real-time quantitative polymerase chain reaction (qRT-PCR). Results are presented as the means \pm standard deviation (SD) from three independent experiments. The results are shown after normalization against the values obtained for COLO-320 cells under the 2D culture (value = 1). DLD-1, CACO-2, and HCT-15 cells had high E-cadherin and low vimentin mRNA levels, whereas SW480 and COLO-320 cells had low E-cadherin and high vimentin mRNA levels in the 2D culture (black bars). DLD-1 cells, which exhibited the highest E-cadherin expression in 2D culture, showed a significant decrease in E-cadherin expression in 3D culture. COLO-320 cells, which had the highest vimentin expression in 2D culture, and SW480 cells, which had the second-highest vimentin expression, both demonstrated significantly decreased vimentin expression in 3D culture (white bar). * $p < 0.05$.

Immunocytochemical and Western blot analyses

Immunocytochemical analysis of cell blocks revealed that E-cadherin was weakly expressed in the cytoplasm of epithelial DLD-1, CACO-2, HCT-15, and mesenchymal SW480 cells in 2D culture, but was strongly localized to the plasma membrane in these cells in 3D culture (Fig. 2, upper two rows, Supplementary figure S2). The localization of vimentin protein in SW480 cells was diffuse in many cells in 2D culture but positive in some clustered cells in 3D culture (Fig. 2, lower two rows, Supplementary figure S2). In COLO-320 cells, vimentin protein expression was observed in the cytoplasm of most cells in 2D and 3D cultures. The E-cadherin and vimentin expression in these CRAC cells were then quantified using Western blotting (Fig. 3, Supplementary figure S3). E-cadherin was expressed in CRAC cells other than the COLO-320 cells, and the expression level was higher in 3D culture than that in 2D culture (Fig. 3, upper panel). In contrast, vimentin was observed in SW480 and COLO-320 cells (Fig. 3, middle panel). The quantitative results of the Western blot corresponded to the staining results of immunocytochemical staining.

Morphological images of CRAC cells in 2D culture

Phase contrast microscopy and scanning electron microscopy (SEM) showed polymorphic cancer cells with microvilli attached to the culture plate and spherical cancer cells with smooth surfaces during cell division (Fig. 4a, b, arrows); however, there were no significant differences in the morphology of the five CRAC types. When CRAC cells were detached from the plates with trypsin, cell blocks were prepared and stained with H&E, CACO-2, and COLO-320 cells had a few cancer cells with atypical large nuclei (Fig. 4c, arrowheads).

Morphological analysis of spheres formed in 3D culture

CRAC cells were cultured on low-attachment plates and the morphology of the spheres formed in the culture medium was observed. Under phase-contrast microscopy, CACO-2 and HCT-15 cells formed small spheres, whereas other CRAC cells produced large, loosely connected, granular spheres (Fig. 5a). SEM revealed that the surfaces of the HCT-15 cell spheres consisted of flattened lining cells and spherical cancer cells (Fig. 5b, c). CACO-2 cells observed by SEM formed a characteristic sphere that resembled a cluster of baseball balls with holes (Fig. 5c, arrowheads). SEM analysis of DLD-1, SW480, and COLO-320 cells revealed spheres consisting of small round cancer cells. Among SW480 cells, several cancer cells adhered to each other, creating a tubular structure with holes (arrowheads). Hematoxylin and eosin (H&E) staining of sphere cell blocks demonstrated that CACO-2, HCT-15, and SW480 cells maintained their spherical morphology (Fig. 5d). In contrast, DLD-

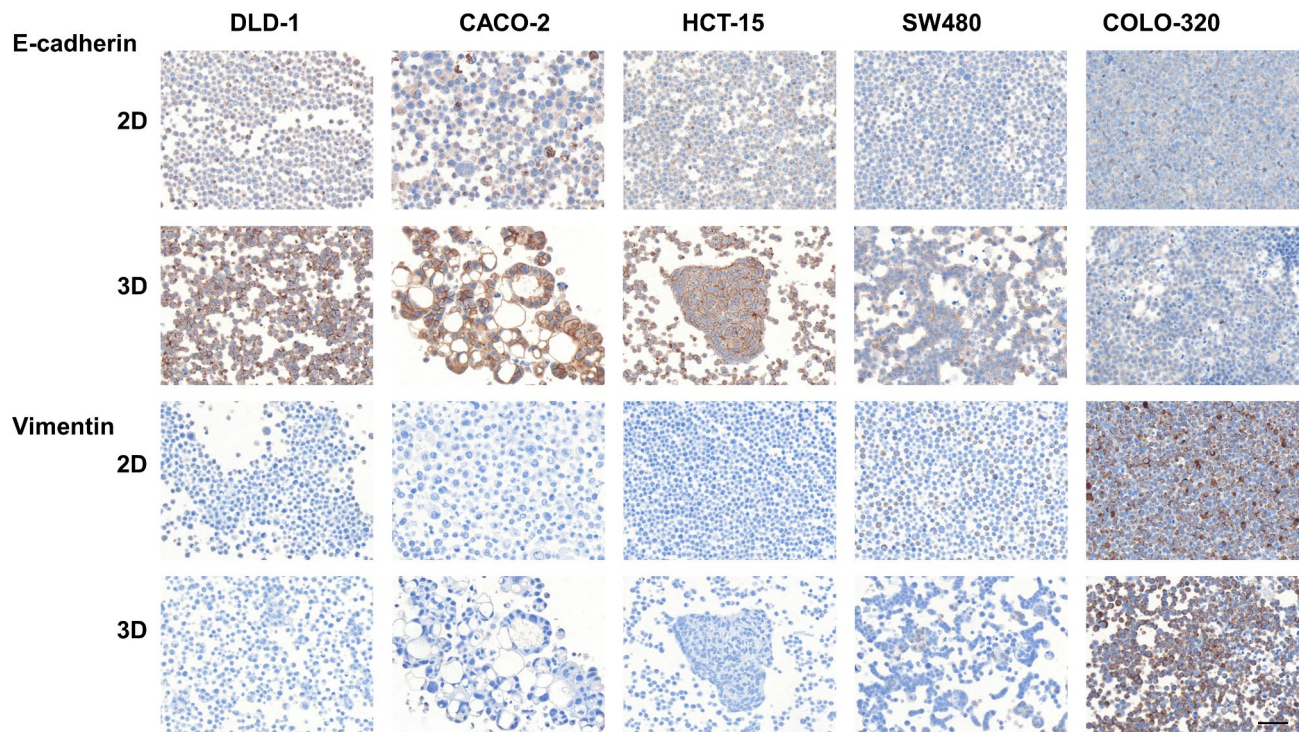


Fig. 2. Immunocytochemical images of E-cadherin and vimentin in 2D and 3D cultured colorectal adenocarcinoma (CRAC) cells. E-cadherin and vimentin expression levels in five human CRC cell lines were determined using immunocytochemical analysis. In 2D cultures, E-cadherin was weakly expressed in the cytoplasm of DLD-1, CACO-2, HCT-15, and SW480 cells, but in 3D cultures it was prominently localized to the plasma membrane in these cells. Vimentin was localized in SW480 and COLO-320 cells cultured in 2D and 3D cultures. Scale bar = 50 μ m.

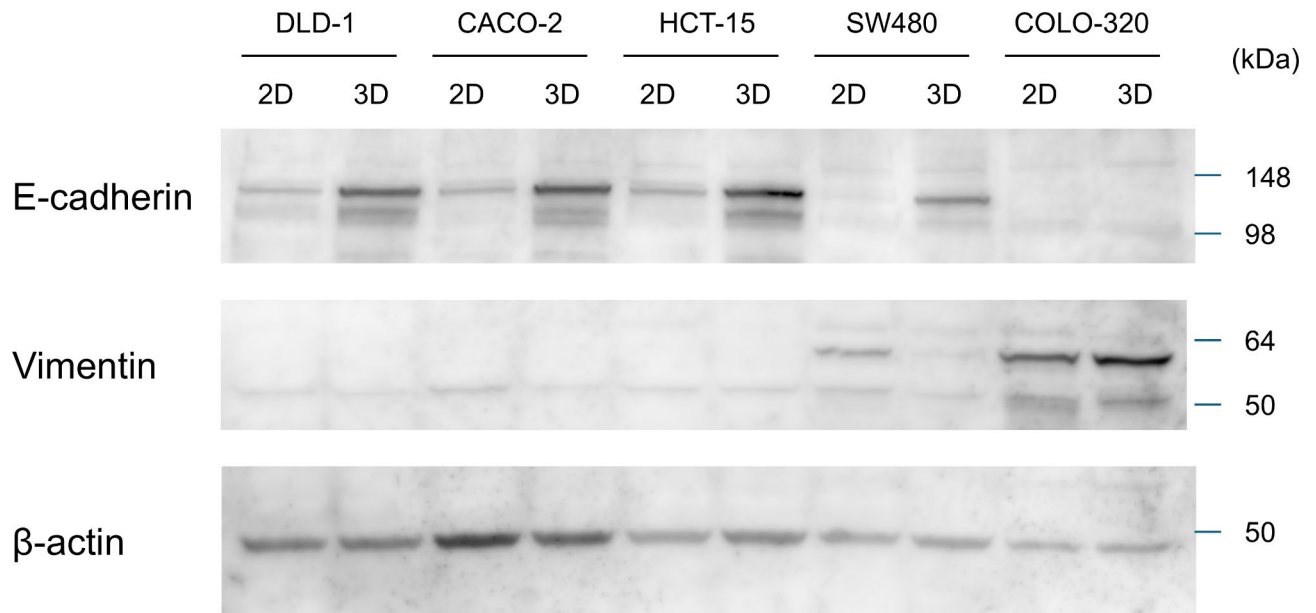


Fig. 3. Western blot analysis of E-cadherin and vimentin in 2D and 3D cultured colorectal adenocarcinoma (CRAC) cells. E-cadherin and vimentin expressions were compared between CARC cell lines cultured under 2D and 3D conditions. E-cadherin was prominently expressed in DLD-1, CACO-2, HCT-15, and SW 480 cell lines, with enhanced expression observed under 3D culture conditions. In contrast, vimentin was expressed in 2D cultured SW480 and in both 2D and 3D cultured COLO-320 cells. β -actin was used as an internal control.

Mew

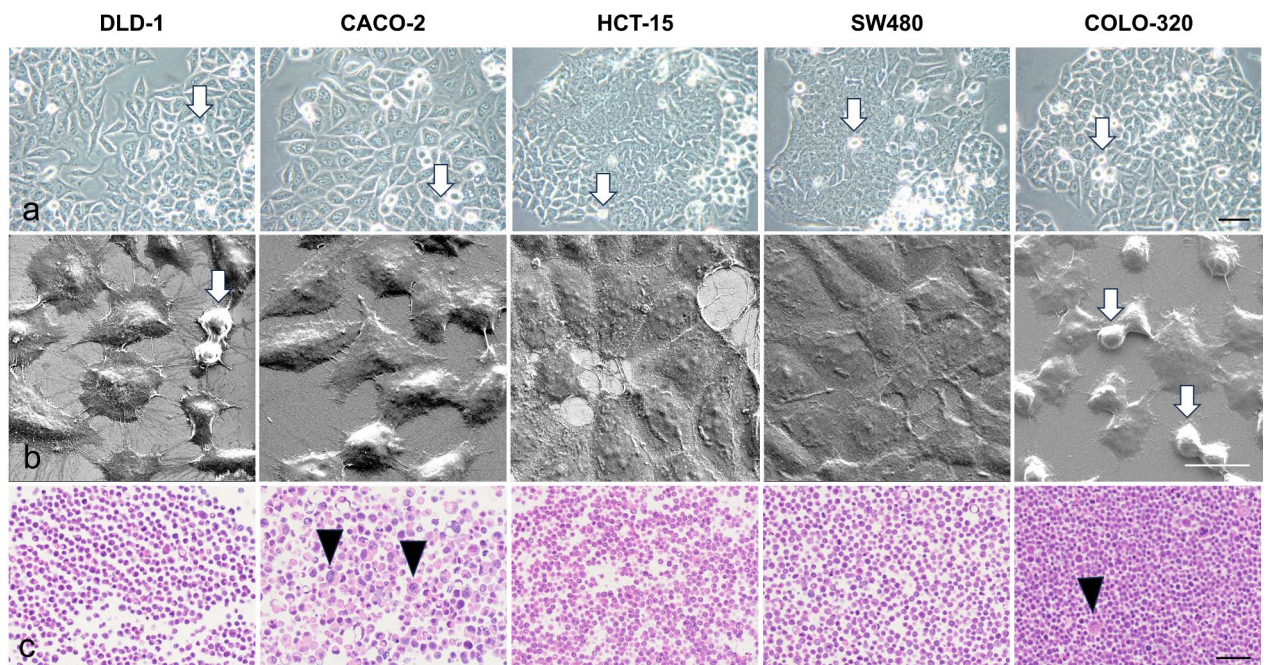


Fig. 4. Characteristic morphological images of colorectal adenocarcinoma (CRAC) cells cultured in 2D culture. **(a)** Phase contrast microscopy showed that CRAC cells exhibited two types of morphology: polymorphic and spherical (arrows), with each cell line exhibiting similar morphology to the other. **(b)** Scanning electron microscopy (SEM) analysis showed that the CRAC cells were polymorphic and had numerous microvilli around the cells, which also adhered to each other. Arrows indicate spherical proliferating cells. **(c)** Examination of hematoxylin and eosin (H&E)-stained cell blocks revealed cancer cells with marked atypical nuclei in CACO-2 and COLO-320 cells (arrowheads) (scale bars: a = 50 μ m, b = 20 μ m, c = 50 μ m).

New

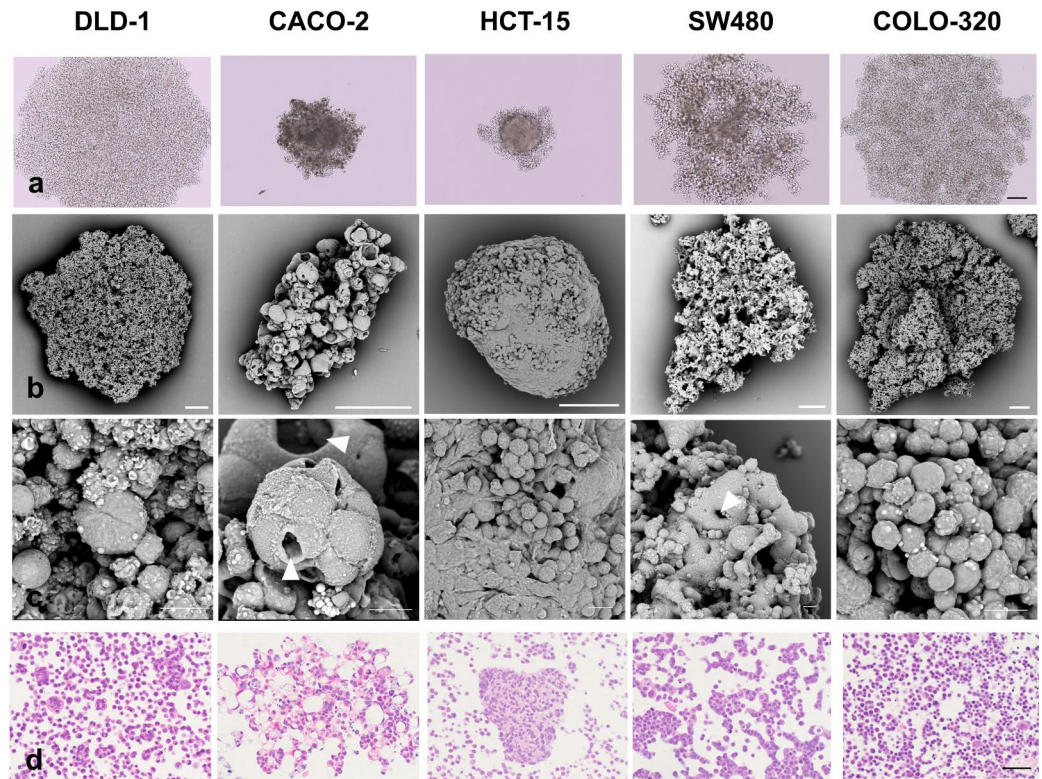


Fig. 5. Characteristic morphological images of colorectal adenocarcinoma (CRAC) cells cultured in 3D culture. Phase contrast microscopy showed that HCT-15 formed small, solid spheres, while the spheres of other CRAC cells were large and loosely clustered cancer cells. **(b and c)** Scanning electron microscopy (SEM) showed that the DLD-1 and COLO-320 cells formed large spheres of individual cancer cells. Spheres of CACO-2 and SW480 cells showed fusion of cells on the surface of the spheres and small holes between them (arrowheads). The 3D CACO-2 were intact spherical structures, and HCT-15 cells formed spherical spheres with flattened coated cells. **(d)** In the hematoxylin and eosin (H&E)-stained cell block, CACO-2, HCT-15, and SW480 cells were mutually bound, while DLD-1 and COLO-320 cells were separated by individual cancer cells (scale bars: a = 200 μm , b = 100 μm , c = 10 μm , d = 50 μm).

1 and COLO-320 cells exhibited loose connections between the cancer cells, leading to cell separation and dispersion.

Transmission electron microscopy (TEM) was performed to study the microstructure of the cross sections of the CRAC spheres. In the spheres formed by DLD-1 cells, cancer cells covered with microvilli were observed (Fig. 6, black arrows) along with intracytoplasmic and intercellular tubular structures lined by microvilli (asterisks) and desmosome-like structures (arrowheads). The spheres of CACO-2 cells contained lysosomes (L) and glycogen granules (G), as well as intracellular and intercellular vacuole formation (white and black circles, respectively). Additionally, microvilli (black arrows) and entosis, where one cell engulfed another, were observed in CACO-2 cells (white arrows). HCT-15 cell spheres exhibit entosis (white arrow), prominent glycogen granules (G), pseudopodia (P), and well-developed desmosome-like structures (arrowheads). Microvilli are observed in SW480 cell spheres (black arrows), along with entosis (white arrows) and tubular structures (asterisks). Tonofibrils were noted within the cytoplasm of SW480 cells (insets, white arrowheads). COLO-320 cell spheres display microvilli (black arrows), prominent pseudopodia (P), and large mitochondria (M). Tubular structures (asterisks) and neuroendocrine granules (N) are also observed in COLO-320 cells.

Table 1 summarizes the characteristics of the CRAC spheres observed using TEM. Microvilli were observed in the spheres of all the CRAC cell types. Pseudopodia were present in epithelial HCT-15 and mesenchymal COLO-320 cells. Tubular structures were observed in epithelial DLD-1, mesenchymal SW480, and COLO-320 cells. Desmosome-like structures were observed in only three epithelial cell lines. Tonofibrils were exclusively observed in the mesenchymal SW480 cells. Neuroendocrine granules were found only in mesenchymal COLO-320 cells. Glycogen granules were found in only three epithelial cell lines, as suggested by the results of PAS staining with or without diastase digestion using cell blocks (Supplementary Figure S4, S5). Entosis was observed in epithelial CACO-2 and HCT-15 cells, as well as in mesenchymal SW480 cells.

Cell proliferation assay

The proliferative capacity of CRAC cells cultured in 2D and 3D environments was assessed by Ki-67 immunohistochemical staining of cell blocks (Fig. 7a). In 2D culture, mesenchymal SW480 and COLO-320

New Figure 6

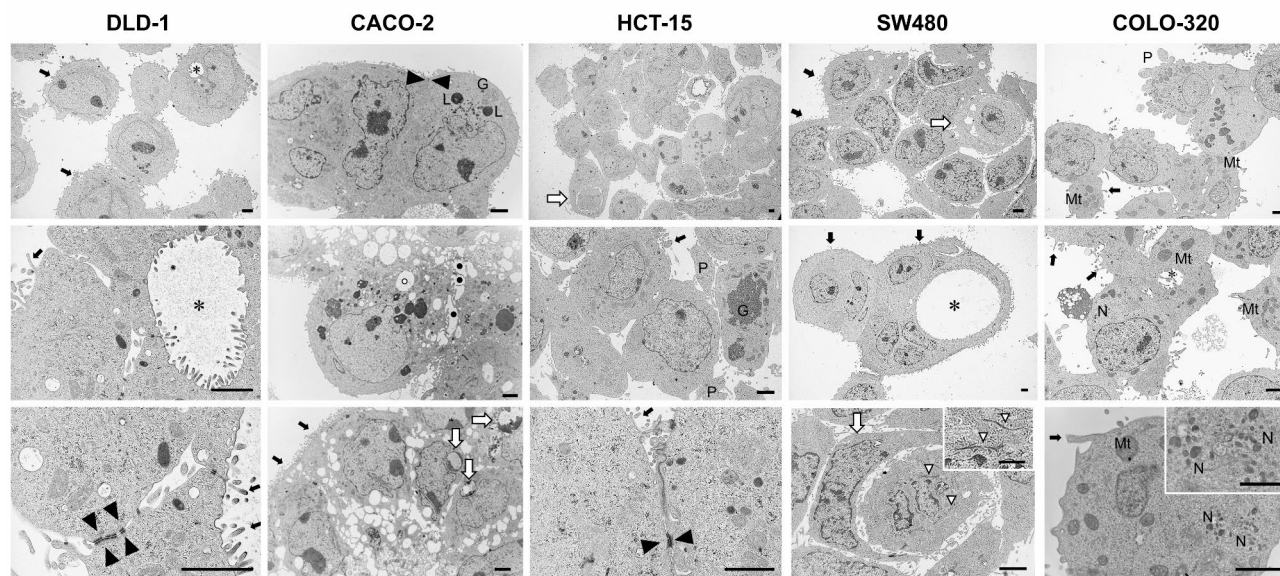


Fig. 6. Transmission electron microscopic (TEM) analysis of 3D cultured colorectal adenocarcinoma (CRAC) cells. All CRAC sphere-forming cancer cells showed numerous microvilli on the plasma membrane (arrows). Desmosome-like structures were found in DLD-1, CACO-2, and HCT-15 cells (arrowheads). Tubular structures are observed in DLD-1, SW-480, and COLO-320 cells (asterisks). Glycogen was detected in the DLD-1, CACO-2 and HCT-15 cells (G). Numerous neuroendocrine granules (N) and large mitochondria (Mt) are found in COLO-320 cells (scale bars: 2 µm; scale bar in inset: 1 µm).

Cell name	Epithelial			Mesenchyma	
	DLD-1	CACO-2	HCT-15	SW480	COLO-320
Microvilli	++	++	++	++	+
Pseudopodia	-	-	+	-	+
Ductal structure	++	-	-	++	+
Desmosome-like structure	++	+	++	-	-
Vacuole	+	++	-	+	-
Tonofibril	-	-	-	+	-
Neuroendocrine granule	-	-	-	-	+
Glycogen	+	++	++	-	-
Entosis	-	+	+	+	-

Table 1. Summary of transmission electron microscopy findings of spheres of colorectal cancer cell lines.

cells exhibited a higher number of Ki-67 positive cells than epithelial DLD-1 and HCT-15 cells (Fig. 7a, b). For epithelial DLD-1 and HCT-15 cells, there was a significantly higher number of Ki-67 positive cells in the 3D cultures than in the 2D cultures (Fig. 7b, $p < 0.05$), whereas the opposite trend was observed for CACO-2 cells ($p < 0.05$). In contrast, mesenchymal SW480 and COLO-320 cells maintained a high number of Ki-67 positive cells in both 2D and 3D cultures (Fig. 7b). These findings suggest that the proliferative capacity of epithelial colorectal cancer cell lines is influenced by culture conditions, such as 2D and 3D, whereas mesenchymal cell lines maintain high proliferative capacity in both 2D and 3D cultures.

Discussion

Growing evidence suggests that the heterogeneity in cancer cell populations is an obstacle to effective cancer treatments. Here, we found that E-cadherin mRNA levels were highly variable among the five CRAC cell lines. DLD-1, CACO-2, and HCT-15 cells exhibited high E-cadherin mRNA levels and significantly reduced vimentin mRNA levels. In contrast, SW480 and COLO-320 cells exhibit low E-cadherin mRNA levels, and increased vimentin mRNA levels. These results are consistent with those of previous studies using PDAC cell lines¹⁸. E-cadherin and vimentin mRNA levels in 2D culture correlated with protein levels, as observed by the immunocytochemical staining of CRAC cells. These findings suggest that CRAC cell lines are heterogeneous and

New

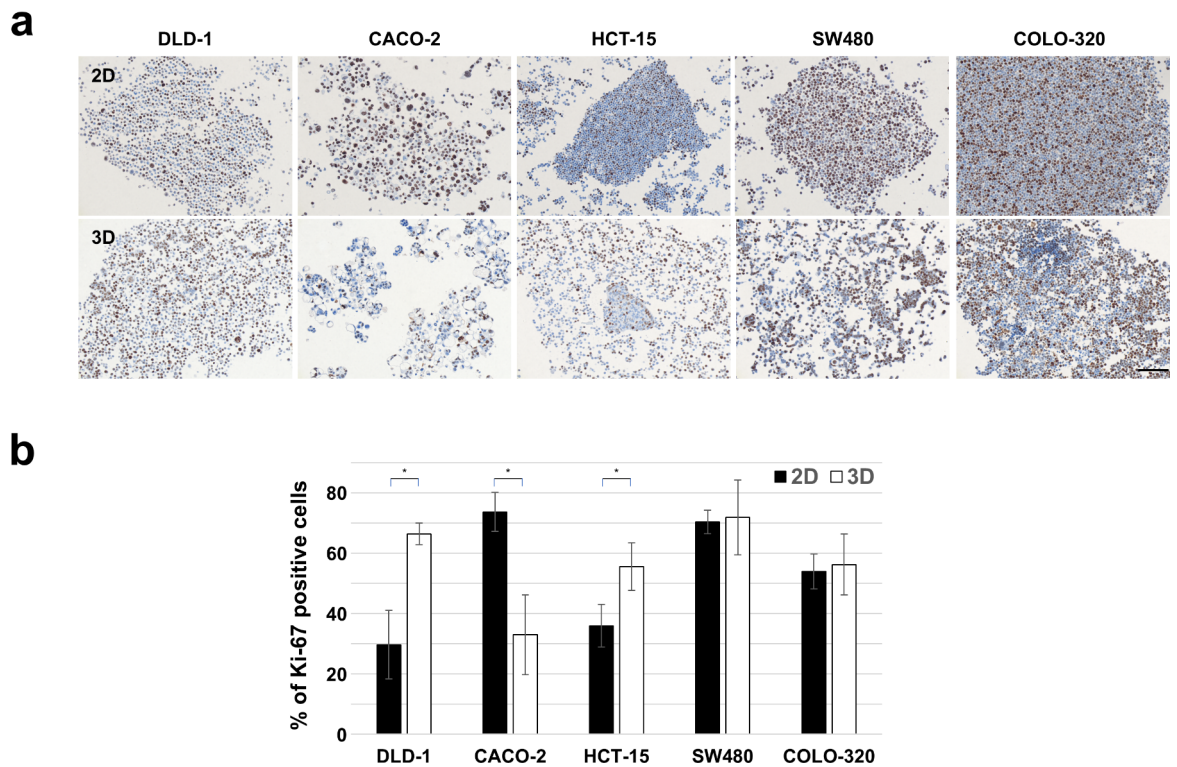


Fig. 7. Analysis of cell proliferation ability. **(a)** Immunocytochemical analysis of Ki-67 in CRC cells under 2D (upper row) and 3D (lower row) culture conditions. Ki-67-positive cells were diffusely present in cancer cells. Scale bar = 100 μm . **(b)** Quantification of Ki-67-positive cells. There were differences in the number of Ki-67 positive cells in 2D and 3D cultures for DLD-1, CACO-2, and HCT-15 cells, but no change in the number of Ki-67 positive cells in SW480 and COLO-320 cells. Data are shown as the mean \pm standard deviation (SD). * $p < 0.05$.

consist of cells with various levels of epithelial and mesenchymal features, indicating the difficulty in removing colon cancer cells by drug treatment.

In our previous 3D culture experiments, PDAC cells with epithelial features formed small and solid spheres with flat-lined cells along the periphery; however, PDAC cells with mesenchymal features formed larger spheres than those with epithelial features with a grape-like appearance and consisted of loosely attached individual cancer cells^{18–20}. In this study, CRAC cell spheres in 3D cultures were not related to epithelial-mesenchymal traits in 2D cultures. Only HCT-15 cells formed spheres similar to those observed in epithelial PDAC cells, whereas other CRAC cells formed large spheres, with individual cancer cells loosely bound together. Therefore, we examined whether the epithelial-mesenchymal traits of CRAC cells in 2D cultures were altered in 3D cultures. Vimentin mRNA expression in SW480 and COLO-320 mesenchymal cells was reduced in 3D cultures, whereas E-cadherin mRNA expression in DLD-1 cells, the epithelial lineage with the highest E-cadherin expression, was decreased. Although these changes were not pronounced at the protein level, they suggested that the culture environment significantly altered the epithelial-mesenchymal traits of CRAC cells. These results suggest that a 3D culture environment, which is more in vivo-like than a 2D culture, may attenuate the strong epithelial and mesenchymal properties of CRAC cells and reduce the differences in CRAC cell lines. To clarify the differences in the epithelial-mesenchymal features of 2D and 3D-cultured CRAC cells, comprehensive studies, such as transcriptome and proteomic analyses, will be necessary in the near future.

With regard to cell proliferative capacity, the three epithelial CRAC cell lines, DLD-1, CACO-2, and HCT 15, showed a significant change in the percentage of Ki-67 positive cells in 3D culture. In contrast, the mesenchymal cell lines SW480 and COLO 320 showed high cell proliferative capacity, which was not affected by the 2D or 3D culture models. Changes in the proliferation rate of epithelial cell lines, but not mesenchymal cell lines, demonstrated that 3D culture affects epithelial cell proliferation only. To reflect the proliferation of CRAC cells in vivo, 3D culture may be an appropriate method to exert their potential.

Epithelial DLD-1 and HCT-15 cells were obtained from the same colon cancer patient. The Cellosaurus, a database of cultured cells, reported similar genetic mutations (Supplementary Table S1). However, DLD-1 and HCT-15 cells showed different E-cadherin expression levels in 2D culture, and the morphology of the spheres formed in 3D culture differed markedly. Tubular structures were observed only in the DLD-1 cells, whereas entosis was observed only in the HCT-15 cells. The diversity among the cell lines isolated from the same patient with CRAC suggests the importance of a 3D culture model for studying colon cancer.

CACO-2 cells exhibit a highly characteristic morphology when cultured in 3D, as observed in this study. A spherical structure resembling a collection of perforated balls was not observed in any of the eight PDAC cell spheres. CACO-2 cells are a human epithelial colon adenocarcinoma cell line commonly used in scientific research, particularly in studies on intestinal absorption and permeability^{22,23}. These cells are derived from human colon carcinoma and spontaneously differentiate into enterocyte-like cells that resemble the characteristics of the small intestinal epithelium when cultured. In addition to their ability to form tight junctions and express a variety of transporters and enzymes found in the intestinal lining, 3D culture, which enhances the morphological traits of CACO-2 cells, may serve as a valuable *in vitro* model for evaluating drug absorption, nutrient transport, and intestinal barrier function in the field of small intestinal epithelium studies.

SW480 cells grown on collagen matrices form branching structures when cocultured with mesenchymal cells²⁴. In the present study, the cells cultured under 3D conditions formed branch-like structures with fused cancer cells and holes in some parts. Our 3D culture model is simple, uses the same medium as a general 2D culture, and does not require any substrates or other cell types. The only difference from the 2D culture conditions is the use of ultralow attachment plates. This simple and effective culture method for the formation of complex steric spheres may be valuable for studying the properties of colon cancer cell lines.

Entosis, the invasion of one living cell into another cell of the same type, has been observed in epithelial CACO-2, HCT-15, and mesenchymal SW480 cell spheres. The frequency of entosis increases in aggressive tumors and is clearly related to tumor grade and metastasis, and correlates with cancer prognosis^{25–29}. Indeed, cell migration assays conducted using the scratch assay showed faster closure in CACO-2 than in DLD-1 cells³⁰. Thus, the presence of a cell-in-cell structure (entosis) in CACO-2, HC-15, and SE480 cells may indicate their higher potency to migrate from the colon to other tissues.

COLO-320 cells, a CRAC cell line, are known for their neuroendocrine properties as they express markers typically associated with neuroendocrine cells, such as chromogranin A and synaptophysin³¹. This makes COLO-320 cells a valuable model for studying neuroendocrine differentiation in colorectal cancer and exploring the mechanisms behind neuroendocrine tumor (NET) development in the colon. Among the spheres of the five CRAC strains cultured in 3D, only COLO-320 showed neuroendocrine granules under TEM. These morphological results further emphasized that this cell line is appropriate for studying NET development in the colon.

In CRAC cases, E-cadherin expression is associated with favorable clinicopathological factors, whereas vimentin expression is the opposite and is associated with lymph node metastasis and poor prognosis^{14,15,32,33}. Since E-cadherin and vimentin expression differ among CRAC cell lines in 2D and 3D cultures, the epithelial-mesenchymal traits of CRAC cells should be considered when used in clinical studies.

Comparing the differences in the effects of anticancer drugs and functions of drug resistance markers between 2D and 3D cultures using this 3D culture method could be useful for elucidating the effects of drugs in the body and requires further investigation. A recent study has demonstrated the importance of co-culturing spheroids of 3D cultured human hepatocellular carcinoma cell lines and fibroblasts in a chamber³⁴. Here, gene expression related to the development, progression, and poor prognosis of hepatocellular carcinoma increased, suggesting the importance of crosstalk between tumors and stromal cells. Our study is an *in vitro* investigation using five CRAC cell lines, and the role of stromal cells remains unclear. In the near future, further studies using three-dimensional co-culture systems with inflammatory cells, fibroblasts, and organoids will be necessary.

In conclusion, a 3D culture of CRAC cell lines altered the epithelial/mesenchymal expression features, cell morphology, and cell proliferative ability (Supplementary figure S6). 3D cultures may play important roles in the functional analysis of colon cancer and in studying the effects of anticancer drugs *in vitro*.

Methods

Cell culture

CACO-2 and COLO-320 human CRAC cells were provided by the RIKEN BioResource Research Center through the National Bio-Resource Project of the Ministry of Education, Culture, Sports, Science, and Technology, Japan³¹. DLD-1, HCT-15, and SW480 human PDAC cell lines were obtained from the Cell Resource Center for Biomedical Research, Institute of Development, Aging and Cancer, Tohoku University (Sendai, Japan)²⁴. The characteristics of the five CRAC cell lines are summarized in Supplementary Table S1. Cells were grown in growth medium (RPMI-1640 medium containing 10% fetal bovine serum) at 37 °C in a humidified 5% CO₂ atmosphere. To form spheres, cells (3×10^3 cells/well) were plated in 96-well ultra-low attachment U-shaped bottom plates (Thermo Fisher Scientific, Waltham, MA, USA) containing growth medium. After 5 d, the spheres were photographed using a phase-contrast microscope (Eclipse TS-100, Nikon, Tokyo, Japan). The spheres were aspirated using micropipettes and used in further experiments (Supplementary Figure S1). Genomic DNA was extracted from CRAC cells using the DNeasy Blood and Tissue Kit (Qiagen, Hilden, Germany) according to the manufacturer's instructions. Short tandem repeats were analyzed using the GenePrint 10 System (Promega, Madison, WI, USA) at BEX Co., Ltd. in accordance with the manufacturer's instructions, and all CRAC cell lines were confirmed to be correctly genotyped and contamination-free (Supplementary figure S7).

Quantitative reverse transcription-polymerase chain reaction (qRT-PCR)

Total RNA was isolated from cells using a NucleoSpin RNA Kit (Macherey-Nagel GmbH & Co. KG, Düren, Germany) and subsequently reverse-transcribed using the SuperScript™ IV VIL0™ Master Mix (Thermo Fisher Scientific). qRT-PCR was performed using the PowerTrack™ SYBR Green Master Mix (Thermo Fisher Scientific) and the QuantStudio 3 real time PCR system (Thermo Fisher Scientific). The F-primer for E-cadherin is (5'-GCC-TCC-TGA-AAA-GAG-AGT-GGA-AG-3'), R-primer is (5'-TGG-CAG-TGT-CTC-TCC-AAA-TCC-G-3'); F-primer for vimentin is (5'-AGG-CAA-AGC-AGG-AGT-CCA-CTG-A-3'), R-primer is (5'-ATC-TGG-CGT-TCC-AGG-GAC-TCA-T-3'); F-primer for GAPDH is (5'-GTC-TCC-TCT-GAC-TTC-AAC-AGC-G-3'),

R-primer is (5'-ACC-ACC-CTG-TTG-CTG-TAG-CCA-A-3'). GAPDH was used as the internal control. The threshold crossing value was noted for each transcript and normalized to that of the internal control. The relative quantification of each mRNA was performed using the comparative Ct method. Gene expression measurements were performed in triplicate.

Cell blocks for adherent cells and spheres

To prepare cell blocks, adherent cells were collected after trypsin treatment, centrifuged at 1,500 rpm for 5 min, and fixed in 10% neutral-buffered formalin for 3 h. The spheres were collected under a microscope using a micropipette and fixed in 10% neutral-buffered formalin for 3 h. Formalin was removed using a micropipette, and the spheres were dehydrated in graded ethanol and embedded in paraffin.

SEM analysis

SEM analysis was performed using previously reported methods³⁵. CRAC spheres were fixed overnight with 2.5% glutaraldehyde in 0.1 M phosphate buffer (pH 7.4) at 4 °C. The glutaraldehyde solution was then removed and the cells were washed with phosphate-buffered saline (PBS). The CRAC spheres were postfixed with 1% OsO₄ for 30 min. After complete dehydration in a graded ethanol series, the samples were suspended in 100% ethanol, air-dried, and coated with a platinum layer using an MSP-1 S sputter coater (Shinku Device, Ibaraki, Japan). The CRAC spheres were examined and photographed using a Phenom Pro desktop scanning electron microscope with reflected electrons for spheres or secondary electrons for cells attached to culture plates (Thermo Fisher Scientific, Waltham, MA, USA).

Immunocytochemical analysis

For sphere formation in 3D culture, CRAC cells in the growth medium were plated at 3.0×10^3 cells/well in 96-well ultra-low attachment plates (Cat. no. 174925, Thermo Fisher Scientific). The spheres were aspirated after 7 d using micropipettes and used for immunocytochemistry. Cell blocks were prepared as previously reported^{18,19,35} with minor modifications. Briefly, CRAC spheres were fixed in formalin for 3 h at room temperature. Formalin was removed using a micropipette and the spheres were dehydrated in graded ethanol and embedded in paraffin. Subsequently, serial sections of the cell blocks (3 µm thickness) were stained using the Histofine Simple Stain Kit (Nichirei Biosciences Inc., Tokyo, Japan). Antigen retrieval was performed using retrieved antigen solutions. The following primary antibodies were used for the immunocytochemical staining: mouse monoclonal anti-E-cadherin (M106; Takara Bio, Shiga, Japan), mouse monoclonal anti-vimentin (422101; Nichirei), and mouse monoclonal anti-Ki-67 antibodies (M1240) from Dako). The sections were then treated with 0.3% H₂O₂ in water at room temperature for 5 min to block endogenous peroxidase activity. Reactions with each antigen were visualized by the addition of 3,3'-diaminobenzidine tetrahydrochloride and counterstaining with hematoxylin. Negative controls were generated by omitting the primary antibodies. Images were captured using a Matra 2 multispectral microscope (PhenoImager Mantra2; AKOYA Biosciences, Marlborough, MA, United States) in 10 random fields at 200 × magnification. The number of Ki-67 positive cells was measured using the measurement function of inForm software (AKOYA Biosciences). For H-score measurement, images were captured using a Matra 2 multispectral microscope. Photographs were then analyzed using inForm 2.4.2 software. The intensity was divided into four categories: negative, weakly positive, positive, and strongly positive, with scores of 0, 1, 2, and 3, respectively. The H-score was calculated by multiplying the percentage of cells exhibiting each intensity. In 2D culture, > 4000 cells were measured in 4 fields of view, and in 3D culture, > 1500 sphere-forming cells were measured in 4 fields of view.

Western blot analysis

CRAC cells cultured in both 2D and 3D conditions were lysed in radio-immunoprecipitation assay (RIPA) buffer supplemented with complete mini protease inhibitor cocktail (Roche Diagnostics K. K., Mannheim, Germany). Equal amounts of proteins (30 µg) were loaded on 12% TGX gel (Hercules, CA, BioRad), separated by SDS-PAGE, and transferred to a PVDF membrane. The membranes were blocked with Intercept TBS Blocking Buffer (LI-COR Environmental, Lincoln, NE) and incubated with anti-human E-cad (HECD-1) mouse monoclonal antibody (1:500, M106, TaKaRa) or anti-vimentin (V9) mouse monoclonal antibody (1:500, MA5-11883, Thermo) overnight at 4 °C. For the loading control antibody, goat anti β-actin antibody (abcam, ab8229) was used. Membranes were washed with TBS (0.05% Tween-20) and incubated with respective secondary antibodies (1:8,000) for 1 h at RT. Bands were visualized with ChemiDoc MP imaging system (BioRad).

TEM analysis

TEM images were acquired as previously reported³⁶. Spheres from CRAC cells were fixed with 2.5% glutaraldehyde in 0.1 M phosphate buffer (pH 7.4), post-fixed for 1 h with 2% OsO₄ dissolved in distilled water, dehydrated in a graded series of ethanol solutions, and embedded in Epon. Ultrathin sections were prepared and stained with uranyl acetate and lead citrate for observation under a transmission electron microscope (H-7500; Hitachi High Technologies).

Statistical analysis

Results are presented as mean ± standard deviation (SD). Data were analyzed using Easy R (EZR; Saitama Medical Center, Jichi Medical University, Saitama, Japan), a GUI for R (R Foundation for Statistical Computing, Vienna, Austria) that adds functions frequently used in biostatistics. Continuous variables were analyzed using Student's t-test. Statistical significance was set at $p < 0.05$.

Data availability

All data generated or analysed during this study are included in this published article and its supplementary information files.

Received: 13 September 2024; Accepted: 21 January 2025

Published online: 24 January 2025

References

- Bray, F. et al. Global cancer statistics 2018: GLOBOCAN estimates of incidence and mortality worldwide for 36 cancers in 185 countries. *CA Cancer J. Clin.* **68**, 394–424. <https://doi.org/10.3322/caac.21492> (2018).
- Vogelstein, B. et al. Genetic alterations during colorectal-tumor development. *N Engl. J. Med.* **319**, 525–532. <https://doi.org/10.1056/NEJM198809013190901> (1988).
- Crockett, S. D., Nagtegaal, I. D. & Terminology Molecular features, epidemiology, and management of serrated colorectal neoplasia. *Gastroenterology* **157**, 949–966 e944, (2019). <https://doi.org/10.1053/j.gastro.2019.06.041>
- Pilleron, S. et al. Estimated global cancer incidence in the oldest adults in 2018 and projections to 2050. *Int. J. Cancer.* **148**, 601–608. <https://doi.org/10.1002/ijc.33232> (2021).
- Sehgal, M. et al. Colorectal cancer incidence after colonoscopy at ages 45–49 or 50–54 years. *Gastroenterology* **160**, 2018–2028 e (2013). <https://doi.org/10.1053/j.gastro.2021.02.015> (2021).
- Peterse, E. F. P. et al. The impact of the rising colorectal cancer incidence in young adults on the optimal age to start screening: Microsimulation analysis I to inform the American cancer society colorectal cancer screening guideline. *Cancer* **124**, 2964–2973. <https://doi.org/10.1002/cncr.31543> (2018).
- Wolf, A. M. D. et al. Colorectal cancer screening for average-risk adults: 2018 guideline update from the American cancer society. *CA Cancer J. Clin.* **68**, 250–281. <https://doi.org/10.3322/caac.21457> (2018).
- Siegel, R. L. et al. Colorectal cancer incidence patterns in the United States, 1974–2013. *J. Natl. Cancer Inst.* **109** <https://doi.org/10.1093/jnci/djw322> (2017).
- Shinji, S. et al. Recent advances in the treatment of colorectal cancer: a review. *J. Nippon Med. Sch.* **89**, 246–254. https://doi.org/10.1272/jnms.JNMS.2022_89-310 (2022).
- Yang, J. et al. Guidelines and definitions for research on epithelial-mesenchymal transition. *Nat. Rev. Mol. Cell. Biol.* **21**, 341–352. <https://doi.org/10.1038/s41580-020-0237-9> (2020).
- Huang, Y., Hong, W. & Wei, X. The molecular mechanisms and therapeutic strategies of EMT in tumor progression and metastasis. *J. Hematol. Oncol.* **15**, 129. <https://doi.org/10.1186/s13045-022-01347-8> (2022).
- Sasaki, N. et al. TGF-beta1 increases cellular invasion of colorectal neuroendocrine carcinoma cell line through partial epithelial-mesenchymal transition. *Biochem. Biophys. Res. Commun.* **30**, 101239. <https://doi.org/10.1016/j.bbrep.2022.101239> (2022).
- Lu, J., Kornmann, M. & Traub, B. Role of epithelial to mesenchymal transition in colorectal cancer. *Int. J. Mol. Sci.* **24** <https://doi.org/10.3390/ijms241914815> (2023).
- Busuioac, C. et al. Aberrant immunohistochemical expression of OCT3/4 and EMT related markers, Vimentin and E-cadherin, is correlated with adverse histopathological features in colorectal adenocarcinoma. *Chirurgia (Bucur).* **117**, 544–555. <https://doi.org/10.21614/chirurgia.2782> (2022).
- Shinji, S. et al. Clinical and biological significance of lymph node micrometastasis in colorectal cancer. *J. Nippon Med. Sch.* **74**, 77–80. <https://doi.org/10.1272/jnms.74.77> (2007).
- Druzhkova, I. et al. E-cadherin in colorectal cancer: Relation to chemosensitivity. *Clin. Colorectal Cancer.* **18**, e74–e86. <https://doi.org/10.1016/j.clcc.2018.10.003> (2019).
- Collisson, E. A. et al. Subtypes of pancreatic ductal adenocarcinoma and their differing responses to therapy. *Nat. Med.* **17**, 500–503. <https://doi.org/10.1038/nm.2344> (2011).
- Minami, F. et al. Morphofunctional analysis of human pancreatic cancer cell lines in 2- and 3-dimensional cultures. *Sci. Rep.* **11**, 6775. <https://doi.org/10.1038/s41598-021-86028-1> (2021).
- Shichi, Y. et al. Enhanced morphological and functional differences of pancreatic cancer with epithelial or mesenchymal characteristics in 3D culture. *Sci. Rep.* **9**, 10871. <https://doi.org/10.1038/s41598-019-47416-w> (2019).
- Shichi, Y. et al. Epithelial and mesenchymal features of pancreatic ductal adenocarcinoma cell lines in two- and three-dimensional cultures. *J. Pers. Med.* **12** <https://doi.org/10.3390/jpm12050746> (2022).
- Shichi, Y. et al. Artificial intelligence-based analysis of time-lapse images of sphere formation and process of plate adhesion and spread of pancreatic cancer cells. *Front. Cell. Dev. Biol.* **11**, 1290753. <https://doi.org/10.3389/fcell.2023.1290753> (2023).
- Yago, T., Yuda, N., Tanaka, M., Iwao, T. & Matsunaga, T. Evaluating intestinal absorption of peptide met-lys-pro in casein hydrolysate using Caco-2 and human iPS cell-derived small intestinal epithelial cells. *Food Res. Int.* **193**, 114831. <https://doi.org/10.1016/j.foodres.2024.114831> (2024).
- Chomanicova, N., Adamickova, A., Valaskova, S., Gazova, A. & Kyselovic, J. Caco-2 monolayer as a model of the intestinal barrier: Permeability of Magnesium salts. *Methods Mol. Biol.* **2835**, 301–306. https://doi.org/10.1007/978-1-0716-3995-5_25 (2024).
- Richman, P. I. & Bodmer, W. F. Control of differentiation in human colorectal carcinoma cell lines: Epithelial-mesenchymal interactions. *J. Pathol.* **156**, 197–211. <https://doi.org/10.1002/path.1711560305> (1988).
- Abodie, W. T., Dey, P. & Al-Hattab, O. Cell cannibalism in ductal carcinoma of breast. *Cytopathology* **17**, 304–305. <https://doi.org/10.1111/j.1365-2303.2006.00326.x> (2006).
- Krajcovic, M. et al. A non-genetic route to aneuploidy in human cancers. *Nat. Cell. Biol.* **13**, 324–330. <https://doi.org/10.1038/ncb2174> (2011).
- Jose, D. et al. Evaluation of cannibalistic cells: A novel entity in prediction of aggressive nature of oral squamous cell carcinoma. *Acta Odontol. Scand.* **72**, 418–423. <https://doi.org/10.3109/00016357.2013.798872> (2014).
- Bansal, C., Tiwari, V., Singh, U., Srivastava, A. & Misra, J. Cell cannibalism: A cytological study in effusion samples. *J. Cytol.* **28**, 57–60. <https://doi.org/10.4103/0970-9371.80736> (2011).
- Song, J. et al. Cell-in-cell-mediated entosis reveals a progressive mechanism in pancreatic cancer. *Gastroenterology* **165**, 1505–1521 e1520, (2023). <https://doi.org/10.1053/j.gastro.2023.08.035>
- Feng, X. et al. Multiple antitumor effects of picropodophyllin in colon carcinoma cell lines: Clinical implications. *Int. J. Oncol.* **40**, 1251–1258. <https://doi.org/10.3892/ijo.2011.1281> (2012).
- Quinn, L. A., Moore, G. E., Morgan, R. T. & Woods, L. K. Cell lines from human colon carcinoma with unusual cell products, double minutes, and homogeneously staining regions. *Cancer Res.* **39**, 4914–4924 (1979).
- Toiyama, Y. et al. Increased expression of slug and Vimentin as novel predictive biomarkers for lymph node metastasis and poor prognosis in colorectal cancer. *Carcinogenesis* **34**, 2548–2557. <https://doi.org/10.1093/carcin/bgt282> (2013).
- Niknami, Z., Muhammadnejad, A., Ebrahimi, A., Harsani, Z. & Shirkoobi, R. Significance of E-cadherin and Vimentin as epithelial-mesenchymal transition markers in colorectal carcinoma prognosis. *EXCLI J.* **19**, 917–926. <https://doi.org/10.17179/excli2020-1946> (2020).
- Al Hrouf, A., Cervantes-Gracia, K., Chahwan, R. & Amin, A. Modelling liver cancer microenvironment using a novel 3D culture system. *Sci. Rep.* **12**, 8003. <https://doi.org/10.1038/s41598-022-11641-7> (2022).

35. Shichi, Y. et al. Multiple cystic sphere formation from PK-8 cells in three-dimensional culture. *Biochem. Biophys. Rep.* **32**, 101339. <https://doi.org/10.1016/j.bbrep.2022.101339> (2022).
36. Shinji, S. et al. A new anorectal melanoma cell line derived from a primary human rectal tumor. *J. Nippon Med. Sch.* **89**, 368–376. https://doi.org/10.1272/jnms.JNMS.2022_89-402 (2022).

Acknowledgements

The authors thank Ms. Yasuko Hasegawa and Mr. Fumio Hasegawa (Tokyo Metropolitan Institute for Geriatrics and Gerontology) for technical assistance. This work was supported by JSPS KAKENHI, Grant Numbers 21K08744, 22K08835, 22K08882, 24K11881 (Grants-in-Aid for Scientific Research C). We would like to thank Editage (www.editage.com) for the English language editing.

Author contributions

S.S., T.A., and T.I. designed the study and wrote the manuscript. Y.O. performed cell culture and electron microscopy experiments. Y.S. and M.F. performed cell culture, immunocytochemical analysis, and PCR. T. Y., A. M., K. U., Y. Y., G. T., T. I., T. M., S. K., K. H., K. T., and H. Y. provided suggestions and ideas for the experiments. All authors reviewed and edited the draft of the manuscript.

Declarations

Competing interests

The authors declare no competing interests.

Additional information

Supplementary Information The online version contains supplementary material available at <https://doi.org/10.1038/s41598-025-87660-x>.

Correspondence and requests for materials should be addressed to S.S.

Reprints and permissions information is available at www.nature.com/reprints.

Publisher's note Springer Nature remains neutral with regard to jurisdictional claims in published maps and institutional affiliations.

Open Access This article is licensed under a Creative Commons Attribution-NonCommercial-NoDerivatives 4.0 International License, which permits any non-commercial use, sharing, distribution and reproduction in any medium or format, as long as you give appropriate credit to the original author(s) and the source, provide a link to the Creative Commons licence, and indicate if you modified the licensed material. You do not have permission under this licence to share adapted material derived from this article or parts of it. The images or other third party material in this article are included in the article's Creative Commons licence, unless indicated otherwise in a credit line to the material. If material is not included in the article's Creative Commons licence and your intended use is not permitted by statutory regulation or exceeds the permitted use, you will need to obtain permission directly from the copyright holder. To view a copy of this licence, visit <http://creativecommons.org/licenses/by-nc-nd/4.0/>.

© The Author(s) 2025